Recombination spectra of Helium-Like Ions

M. A. Bautista and T. R. Kallman

Laboratory for High Energy Astrophysics

NASA Goddard Space Flight Center

Greenbelt, MD 20771, USA

Received _____; accepted _____

ABSTRACT

We calculate the recombination spectra of the He-like ions He I, C V, N VI, O VII, Ne IX, Mg XI, Si XIII, S XV, Ar XVII, Ca XIX, and Fe XXV. We include the following physical processes: radiative recombination, dielectronic recombination, three-body recombination, electron impact ionization, and collisional excitation by electrons, protons, and α-particles. The calculations also account for the effects of lowering of the continuum at high densities and high density corrections to dielectronic recombination.

From the populations of all levels in the recombined ions we construct models for He-like ions for fast computation of their spectra. Every model includes 29 bound levels up to n=5, a pair of "superlevels" which accounts for radiative and collisional cascades from highly excited levels, 6 doubly excited levels that account for the most important satellite lines, and a level that represents the hydrogenic recombining ion. The models are constructed in a way that allows for proper approach to LTE under appropriate conditions. These models can simultaneously solve for the H/He-like ionization balance in photoionized or collisionally ionized plasmas and compute emission spectra including the combined effects of radiative and dielectronic recombination, collisional excitation, photoionization from excited levels, fluorescence, and line trapping. The models can be used for any temperature between 100 and 10^9K and electron densities of up to 10^{18} cm^{-3} . The models can be easily used within spectral modeling codes or as stand-alone tools for spectral analysis.

We present comparisons between the results of the present models and previous work. Significant differences are found between the present effective recombination rate coefficients to the $n = 2$ and those of previous estimates. Later, we study various emission line ratio diagnostics under collisional

ionization and photoionized conditions.

Subject headings: atomic processes – line formation – X-rays:spectroscopy

1. Introduction

Spectral lines from He-like ions are prominent throughout the electromagnetic spectrum. He I is responsible for many lines in the optical and infrared spectra and they are commonly observed in nebular plasmas. Thus, the low temperature recombination spectrum (without dielectronic recombination) of He I has been extensively studied for over four decades (Mathis 1957; Burgess & Seaton 1960a,b; Pottasch 1961; Robbins 1968, 1970; Robbins & Robinson 1971; Brocklehurst 1972; Bhatia & Underhill 1987; Almog & Netzer 1989; Smits 1991, 1996; Hummer & Storey 1998; Benjamin, Skillman & Smits 1999). The tabulated results from these calculations have then been extensively used in the analysis of observed spectra. Alternatively, a few models for the HeI system have been constructed, based on the treatment by Cota (1987), for implementation into plasma modeling codes (e.g. CLOUDY by Ferland 1986; ION by Netzer 1987; XSTAR v.1 by Kallman & Krolik 1995).

The emission from He-like ions other than He I is important in the X-ray spectra of astronomical and laboratory plasmas. Although the spectral lines from these ions that result from the n=2 levels have received much attention the treatment of recombination excitation has alway been approximated, while no detailed calculation of these ions recombination spectra has been reported. The theory for computing the line intensities for transitions from the n=2 levels in coronal plasmas was developed by Gabriel & Jordan (1969, 1970, 1972, 1973). This theory includes a treatment of dielectronic recombination contributions in addition to collisional excitation. The next major advance in the subject was made by Mewe & Schrijver (1978a,b,c) who introduced approximated treatments for dielectronic and radiative recombination, collisional excitation, and inner-shell ionization. All of this was based on poorly known atomic data which they fit according to ionic nuclear charge along the whole isoelectronic series. Pradhan (1985) studied again the emission from n=2 states

paying special attention to recombination contributions to the emission in non-coronal plasmas. Thus, most currently available spectra modeling codes simply extrapolate effective recombination rates for any He-like ion from the He I rates using hydrogenic scaling rules.

There are at least two other difficulties with available He-like emission models and calculations. One is that all of them are restricted to densities less than 10^{14} cm^{-3}. Yet, various kinds of astronomical X-ray sources of interest could be much denser, for example low-mass X-ray binaries (Bautista et al. 1998) and accretion disks near extragalactic black holes (Nayakshin, Kazanas, and Kallman 2000). The other difficulty is that none of the calculations and models correctly approach LTE under proper conditions. This invalidates those results in the presence of strong radiation fields and in nearly optically thick plasmas.

In the present paper we start by presenting the atomic data used for the calculation. Then we described the calculations of level population and recombination spectra. In Section 4, we explain how the recombination-collisional-radiative models were constructed. In Section 5 we compare the present models and their results with previous work. Finally, our conclusions are presented in Section 6.

2. Atomic Data for He-like ions

In this section we describe the atomic data used in the present work. It is important to note that all of the present calculations are carried out in LS coupling since fine-structure recombination rate coefficients are unavailable. The LS approximation is expected to be accurate as long as Δn=0 radiative transitions are small and relativistic effects in the photoionization cross sections and radiative transition rates remain small. Although the present LS calculations are expected to be accurate additional work is currently in progress to compute the atomic data necessary for fine structure recombination calculations.

2.1. Energy levels and line wavelengths

Term energies and line wavelengths are taken from the compilation of the National Institute of Standards and Technology (Martin, Sugar, and Musgrove 1999) when available. Energies for other $l \leq 2$ terms are from the TOPbase. Energies for $l > 2$ terms not known experimentally are assumed as hydrogenic.

2.2. Photoionization cross sections and recombination rates

We use the photoionization cross sections for n$\leq$ 10 and $l \leq 2$ of Fernley, Taylor, & Seaton (1987) calculated as part of the Opacity Project (OP hereafter; Seaton 1987) and which are available from TOPbase (Cunto et al. 1993). In principle one could obtain total, radiative and dielectronic, recombination rate coefficients by means of the Milne relation using cross sections that resolve all autoionizing resonances. There are, however, some limitations in the OP cross sections: (1) the cross sections are tabulated with an energy mesh too coarse to properly resolve the resonances. In fact, the number of points in the tabulated cross sections is so limited that even the radiative recombination rates cannot be computed with accuracy better than $\sim$5%; (2) The He I cross sections do not contain all contributing series of resonances, and the cross sections for other ions do not include any resonances at all; (3) the OP cross sections for He I are total cross sections, including photoionization into the n=2 states of the hydrogen target ion. However, under most conditions the bulk of the recombining ions are in the ground state, so the calculation of recombination rates should only use state specific photoionization cross sections to the ground state of the target ion.

To solve these problems with the OP He I cross sections we remove the resonances by interpolation between points on opposite sides of the resonances. Later, we truncate

the cross sections at the energy points right before the first n=2 target threshold and extrapolate the cross sections to higher energies using the quantum defect method of Peach (1967). In doing so, these quantum defect high energy cross sections are scaled to match the OP cross sections at the crossing point.

For levels with n> 10 and $l \leq 2$ we use cross sections from the quantum defect method. For all levels with $l > 2$ hydrogenic cross section from the method of Burgess and Seaton (1960a) were used.

The state specific dielectronic recombination (DR) coefficients for n≤ 10 and $l \leq 4$ were taken from ADAS (Badnell et al. 1995). These ADAS rate coefficients are given in tabulated form at temperatures between $(Z-1)^2 \times 10^3$ and $(Z-1)^2 \times 10^4$K which we fit with an expression of the form

$$\alpha_{DR} \times T^{3/2} = \sum_i \tau_i \exp\left[(\epsilon_i - \epsilon_T)/kT\right], \quad (1)$$

for $i \leq 4$. Here, ϵ_T is the ionization energy of the ion and ϵ_i represents the energy of the autoionizing resonance i. The choice of such an expression and the values of τ_i and ϵ_i to fit the DR coefficients are explained is Section 4.1. The resulting fits to the ADAS data are accurate to better than 1% in all cases.

The DR coefficients for $n > 10$ were estimated by n^{-3} extrapolation of the coefficients for lower n. DR coefficients for states with angular momentum, l, greater than 4 are expected to be very small and are neglected altogether.

2.3. Radiative transition probabilities

The TOPbase data provides oscillator strengths, f, and transitions probabilities, A, for $n \leq 10$ and $l \leq 2$ for He-like ions. These transition probabilities are generally accurate to within a few per cent. For He I more accurate data was calculated by Kono and Hattori

(1984). Recently, Nahar and Pradhan (1999) computed fine structure f-values for Fe XXV. Their results when summed over fine structure agree well with the TOPbase data.

For $n > 10$ the A-values were computed using the Coulomb approximation methods described in Smits (1991).

Transition probabilities for the forbidden, $2\ ^3S - 1\ ^1S$, and intercombination, $2\ ^3P - 1\ ^1S$, transitions were taken from Mewe and Schrijver (1978a), which are based on computations by Drake (1969, 1971a, 1971b), Johnson and Lin (1974), and Drake and Dalgarno (1969).

2.4. Collision strengths

We adopt collisional data recommended by Dubau (1994) and Kato and Nakazaki (1989). These reviews consider data for levels up to $n = 5$ at most. Collisional rates for other n changing transitions were calculated using the impact parameter method (Seaton 1962). Rates for angular momentum changing transitions by collisions with electrons, protons, and alpha particles were computed using the impact parameter method but with the modifications suggested by Hummer and Storey (1987).

2.5. Collisional ionization and three body recombination

Collisional ionization rates for excited levels are computed by using the semi-empirical formula by Sampson and Zhang (1988). This formula is based on extensive Distorted Wave calculations of collisional excitation and is expected to be accurate for the He-like ions. However, the formula neglects the contributions of collisional excitation-autoionization which, in the case of ionization from the ground state, sometimes dominate the ionization

rate. Unfortunately, there is no data for excitation-ionization from excited levels. Thus we estimate that collisional excitation rates from excited states may have uncertainties of around 50%. Three body recombination rates are obtained from the collisional ionization rates by means of detailed balance.

$$\alpha_{3B} = \frac{w_i}{w_{i+1}} \frac{1}{2} \left(\frac{h^2}{2\pi m k T} \right)^{3/2} e^{I_i/kT} C_{i\infty}. \tag{2}$$

were $C_{i\infty}$ is the collisional ionization rate coefficient, w_i and w_{i+1} are the statistical weights of the recombined and recombining ions, I_i is the ionization energy of the i state.

3. Calculation of Level Populations

Under ionization-excitation equilibrium conditions the population of any level n_i is given by

$$n_i[\sum_{i \neq i}(A_{ij} + N_e C^e_{ij} + N_p C^p_{ij}) + + N_e Q_{i\infty}] \quad = \sum_{k<i} n_k A_{ki} + \sum_{l<i} n_l (N_e C^e_{li} + N_p C^p_{li}) \\ N^+ N_e \alpha_i + N^+ N_e^2 C_{\infty i}$$

where A_{ij} is the radiative transition rate from level i to level j. N_e/N_p and C^e_{ij}/C^p_{ij} are the density per unit volume of electrons/protons and the transition rates by collisions with electrons/protons respectively. N^+ is the density of the next ionization stage of the element, i.e. the H-like ionic state in this case. α_i is the rate coefficient for recombination (radiative plus dielectronic) to level i. $C_{i\infty}$ and $C_{\infty i}$ are the collisional ionization and 3-body recombination rate coefficients respectively. In principle, the sums in this equation includes energy levels 1 through infinity. However, in the present calculation it was found sufficient to explicitply include levels up to $n = 50$ only, while cascades from higher levels were accounted for by extrapolation.

This recombination-collision-cascade problem was solved with the matrix condensation technique (Burgess and Summers 1976) using the computer code developed by Smits (1991).

The population of all levels up to n=50 of every ion were calculated for several temperatures covering the entire range between 10^3 and 10^9K and nine electron densities from 10^2 to 10^{18} cm^{-3}.

The high density calculations required special attention to account for the effects of lowering of the continuum and suppression of dielectronic recombination. The treatment of these high density effects is described next.

3.1. High density lowering of the continuum

The lowering of the continuum effect is very important under the high plasma densities considered here. This effect comes about from cutting the high-n orbitals of ions due to particle packing, Debye shielding, Stark broadening, and collisional broadening. Under the conditions of interest here particle packing is the most important of these mechanisms. Particle packing occurs when the mean inter-nuclear separation in the plasma is smaller than the distance from the nucleus to the high-n ionic orbitals. By comparing the mean inter-nuclear separation in the plasma with the mean size of ionic orbitals of principal quantum number n, one can define a continuum level as (Hahn 1997):

$$n_P = (1.8887 \times 10^8 z/N^{1/3})^{1/2}, \tag{3}$$

where z is the nuclear charge of the ion considered and N is the density of nuclei in the plasma in cm^{-3}.

Debye shielding is the mechanism by which high-n orbitals are shielded from the electrostatic attraction to the nucleus by a high density of free electrons. According to this mechanism the continuum level is given by (Hahn 1997):

$$n_D = 2.6 \times 10^7 z^2 (T_e/N)^{1/4}, \tag{4}$$

where T_e is in Kelvin and z effective charge if the ion (i.e. $z = Z - 1$ for He-like ions).

Under a high concentration of singly charged ions in a plasma a micro-electric-field is formed which will lead to Stark broadening of the atomic levels. Then, for sufficiently high n-numbers the atomic levels will merge with each other lowering the continuum. In this case the continuum level is given by (Inglis & Teller 1939):

$$n_S = [1.814 \times 10^{26} z^6/N]^{2/15}. \quad (5)$$

For temperatures lower than 10^5 Kz^2/n free electrons contribute to the broadening through the static Stark effect. So the density N in the last equation should include both positive and negative charges. At higher temperatures the electrons contribute to the broadening by means of collisions, but this is smaller than the Stark effect of the same electrons at lower temperatures. Thus, only positive charges are considered in this case.

Furthermore, one may define n_C as the minimum of n_P, n_D, and n_S. Then, only orbitals with $n < n_C$ may be treated as bound, while orbitals with $n > n_C$ are mixed with the continuum and must be excluded from the calculation of the recombination process. One can see that in the case of hydrogen like oxygen (z=8), for example, under conditions of T=10^5 K and N= 10^{16}cm^{-3} only levels with $n \leq 83$ are bound, at $N = 10^{18}$ cm^{-3} only levels with $n \leq 38$ are bound, and at $N = 10^{20}$ cm^{-3} only levels with $n \leq 18$ are bound.

3.2. High density suppression of dielectronic recombination

The effects of high electron densities and radiation fields on DR were studied by Burgess and Summers (1969). DR occurs by means of three basic processes:

(1) Resonance capture, autoionization: $X^{+z}(i) + e^- \leftrightarrow [X^{+(z-1)}(j, nl)]$;

(2) Stabilization: $[X^{+(z-1)}(j, nl)] \rightarrow X^{+(z-1)}(i, nl) + h\nu$;

(3) Cascade: $X^{+(z-1)}(i,nl) \rightarrow X^{+(z-1)}(i,n'l') + h\nu$;

where the brackets indicate an autoionizing state.

Under low electron density conditions the cascade process proceeds until the $X^{+(z-1)}$ ion reaches its ground state, so that the recombination rate is just the total rate of all stabilizations.

High electron densities may affect the reactions (1), (2), or (3) as follows:

(a) The autoionizing states of the recombined ion, $[X^{+(z-1)}(j,nl)]$ in the right hand side of (1), could be affected by collisions with electrons. This would cause a redistribution among the different l-states, leading to an increase in the recombination rate coefficient.

(b) Collisional deexcitation could assist the stabilization (process (2)) which would enhance the DR rate.

(c) Collisional ionization could reduce the number of bound states involved in stabilization process ($X^{+(z-1)}(i,nl)$ in (2)). In other words, the lowering of the continuum effect, discussed in the previous section, will suppress DR in similar fashion as it reduces the total radiative recombination rate.

For the range of densities considered here, $N_e \leq 10^{18}$ cm^{-3}, the effects (a) and (b) can be neglected. This is because collisional transition rates, normally of the order of $N_e 10^{-5}/T_e^{1/2}$, have to compete with the much greater autoionization rates, of order 10^{15} s^{-1}. Furthermore, the net effect of high electron densities considered here is to suppress DR. This has been calculated for some ions by various authors (e.g. Burgess and Summers (1969) and Summers 1972). On the other hand, Jordan (1969) computed an empirical correction factors to DR as function of the maximum bound orbital of the ion before the continuum. This approach allowed Jordan to calculate ionization balance in dense plasmas in good agreement, $\sim 5\%$, with the more elaborate computations of Summers (1972). We

adopt Jordan's method to compute DR suppression factors.

4. Ionization-excitation-spectra models

The computed level populations of the He-like ions that were obtained for density vs. temperature grids allow us to construct ionization-excitation-spectra (IES) models for each ion. These models are capable of simultaneously calculating the H/He-like ionization balance and the line emissivities under a variety of conditions. Our models are similar to those described for the He I case by Cota (1987), Almog and Netzer (1989) and Benjamin, Skillman, and Smits (1999). However, several improvements have been made with respect to those models to allow for accurate treatment of high densities, optical depth effects, and convergence towards LTE.

Cota (1987) and Almog and Netzer (1989) explicitly consider a finite number of levels up to $n = n_{max}$ and adopt four fictitious levels that account for all more excited levels. The recombination cascades from the fictitious levels to the explicit levels are accounted for by using averaged radiative transition probabilities weighted by the level population, which are assumed to be in LTE. This assumption introduces errors in the calculated spectrum, particularly at low temperatures. In the model of Benjamin et al. (1999) cascades from levels with $n > n_{max}$ to the lower are summed over to define "indirect" recombination rates which are fit over a temperature range. This approach avoids the use of fictitious levels and yields higher accuracy under some conditions. However, the method of Benjamin et al. introduces new problems when considering optical depth effects. Let us consider for example a model with indirect recombination rates computed under optically thin conditions (Case A). When using this model to solve the Case B problem one would shut down all transitions to n=1. Then, the total recombination obtained this way would be the total Case B recombination minus the fraction of recombination into $n > n_{max}$ which

cascades down to n=1. For even greater optical depths which affect transition to n=2,3, etc. the error in the total recombination rate obtained by the Benjamin et al. approach will become worse.

Our ionization-excitation model for He-like ions consists of all spectroscopic LS terms with n≤5 (i.e. 29 levels), 2 so called "superlevels", a level that represents the ground state of the H-like ion, and 6 doubly excited levels ($2s^2\ ^1S, 2s2p\ ^1P^o,^3P^o$, and $2p^2\ ^1D,^1S,^3P$).

The superlevels are meant one for the singlets and one for the triplet states and are built to account for all $5 < n \leq 50$ levels. To do that we define:

- recombination rates (RR+DR and three body recombination), α_s:

$$\alpha_s = \sum_m \alpha_m,$$

- radiative transition probabilities, $A_{s\rightarrow i}$:

$$A_{s\rightarrow i} = \frac{\sum_m N_m A_{m\rightarrow i}}{\sum_k N_k},$$

- collisional deexcitation rates, $C_{s\rightarrow i}$:

$$C_{s\rightarrow i} = \frac{\sum_m N_m C_{m\rightarrow i}}{\sum_k N_k}.$$

Here, the sums include all levels with $5 < n \leq 50$, N_m represents the population of the level m which is known from the recombination calculation described in Section 3. All of these rates for transitions involving the superlevels were computed for every pair of points in the temperature vs. density grid. From these values the transition rates at any temperature and density of interest can be obtained with accuracy of approximately 2% by linear interpolation. In addition, all the inverse processes to these rates are calculated by means of detailed balance.

It is important to notice that by separating the collisional and radiative cascades from the superlevels one can correctly treat the problem of high density and high optical

depth where radiative decays from excited levels may be suppressed by self-absorption but cascades still occur via collisional deexcitation.

The doubly excited levels in the IES models were included to account for the most important satellite lines to H-like Lyα emission. Excitation energies, line wavelengths, radiative transition probabilities and autoionizing rates were taken from Vainshtein and Safronova (1978). We also included electron impact excitation rates from bound to doubly excited levels and between doubly excited levels from the calculations of Sampson, Goett, and Clark (1983) and Goett, Sampson, and Clark (1983).

Explicit treatment of doubly excited levels introduces the additional practical complication that these levels will contribute to the DR to the bound levels. Thus, these DR contributions had to be subtracted from the total DR to each bound level as taken from the ADAS database (Badnell et al. 1985). On the other hand, the detailed treatment of doubly excited levels tends to improve the behavior of the models at high densities. This is because by considering collisional transitions involving these levels one accounts for the effects of redistribution of l states and collisional assisted stabilization in the DR process (see Section 3.2). In addition, collisional excitation from bound to doubly excited levels results in excitation-autoionization contributions to the collisional ionization rates which are missing in the rates of Sampson and Zhang (1988).

It is important, however, to be cautious about the predictions of satellite lines due to the large uncertainties in some of the current atomic data, particularly of the collisional rates for doubly excited levels which are based on Coulomb-Born-Exchange collision strengths that neglect resonances. These resonances can dominate the collisional rates for doubly excited levels. For example, Bautista (2000) recently showed that in the case of doubly excited levels of Fe XVI the resonances in the collision strengths would enhance the excitation rates by up to three orders of magnitude. Furthermore, improved calculations

of collision strengths and radiative and autoionization rates for He-like ions are currently underway.

4.1. Convergence to LTE

One important feature of the present IES models is their ability to converge to LTE under appropriate condition. This characteristic is essential if they are to be applicable to conditions of dense plasmas and/or high radiation fields.

For an IES model to properly converge to LTE every transition rate must be balanced by its detailed balance inverse. In the present models the transitions rates of interest and their inverse are:

$$\begin{aligned} \textit{collisional deexcitation} &- \textit{collisional excitation cross sections}, \\ \textit{spontaneous transition probabilities} &- \textit{induced transition probabilities}, \\ \textit{three}-\textit{body recombination} &- \textit{collisional ionization cross sections}, \\ \textit{recombination } (RR+DR) &- \textit{photoionization cross sections including} \\ & \quad \textit{autoionizing resonances}. \end{aligned}$$

The collisional and radiative transition rates are readily balanced from the effective collision strengths, Υ, and A-values. Three-body recombination and collisional ionization balance each other through Eqn.(2). The balance between recombination (RR+DR) and photoionization is somewhat more complicated to achieve due to the fact we have only background photoionization cross sections (i.e. without autoionizing resonances). These cross sections balance only the RR component of the total recombination. To balance DR one needs to work backwards from the DR rates to find at least the dominant autoionizing resonances.

Let us consider a photoionization cross section with zero background and narrow

autoionizing resonances which can be approximated by delta functions at photon energies ϵ_i, i.e.

$$\sigma(\epsilon) = \sum_i a_i \delta(\epsilon - \epsilon_i). \tag{6}$$

From this cross section and using the Milne relation the recombination rate is

$$\alpha = \frac{w_z}{w_{z-1}} \sqrt{\frac{2}{\pi}} \frac{h}{c^2} \frac{1}{(m_e kT)^{3/2}} \sum_i a_i \epsilon_i^2 \exp\left[-(\epsilon_i - \epsilon_T)/kT\right], \tag{7}$$

where w_z and w_{z-1} are the statistical weights of the recombined and recombining levels respectively and ϵ_T is the ionization threshold energy. This equation is equivalent to Equation (1), used to fit the ADAS DR rates, if one defines

$$\tau_i \equiv \frac{w_z}{w_{z-1}} 1.167 \times 10^{-10} \epsilon_i^2 a_i, \tag{8}$$

for ϵ_i in Ryd and a_i in Mb. The choice of the location of the autoionizing resonances comes from the realization that the most prominent resonances are those that belong to the Rydberg series converging to the n=2 states of the H-like recombining ions. These thresholds are located at energies of $Z^2(1 - 1/4)$ Ryd above ϵ_T. Thus, the resonances are approximately $(Z-1)^2/\nu$ Ryd below the threshold, with ν=2, 3, 4, 5, ... Thus,

$$\epsilon_i - \epsilon_T = \frac{3}{4} Z^2 - \frac{(Z-1)^2}{(i+1)}. \tag{9}$$

In practice, we found that at most four resonances are needed to fit the ADAS DR rates to an accuracy better than 1%. Then, these resonances were added to the background photoionizations cross section in order to guarantee that the models converge to LTE under proper conditions.

5. Results

The present section reports the results of the present IES models. We start by comparing our effective recombination coefficients with other calculations. Then we focus

on the case of coronal ionization equilibrium and discuss various line ratio diagnostics for optically thin plasmas. Finally, the spectra from photoionized plasmas is discussed.

5.1. Recombination to n=2 terms

Figs. 1(a)-(b) show the effective recombination rate coefficients (direct recombination and cascades) vs. temperature for the n=2 terms 2 ^3S, and 2 $^3P^o$ respectively. The rates are shown for various He-like ions (O VII, S XV, and Fe XXV). Also in the same figures we show the rate coefficients from Mewe and Schrijver (1978a).

One can see from these figures that the present recombination rates differ significantly from those of Mewe and Schrijver. Particularly problematic is the high temperature where recombination is dominated by DR. Here the discrepancies between Mewe and Schrijver and the present calculation can exceed a factor of four.

Also problematic are the recombination coefficients of Mewe and Schrijver for the 2 ^1S state which are systematically overestimated by a factor of ~ 3. This is shown in Fig. 2 (upper-left panel). Confirmation about the Mewe and Schrijver coefficients being overestimated can be obtained from the He I case. At T=10^4K the direct recombination rate coefficient to 2 ^1S is 5.55×10^{-15} cm^{-3}s^{-1} (see Osterbrock 1989 and Benjamin et al. 1999) and our present total rate coefficient, including cascades, to this state is 6.55×10^{-15} cm^{-3}s^{-1}, which is 16% lower than sum of "direct" and "indirect" recombination rates of Benjamin et al.. On the other hand, the Mewe and Schrijver is 1.99×10^{-14} cm^{-3}s^{-1} which is clearly too high by a factor of 3.

Fig. 2 presents the effective recombination coefficients for n=2 terms against ionic nuclear charge (Z) for temperatures of $10^4 \times (Z-1)^2$ K and low electron density. Also in this figure, are the results of Mewe and Schrijver (solid curves) and the hydrogenic

extrapolation with $(Z-1)$ from neutral helium (dashed curves), i.e.

$$\alpha(T,Z) = (Z-1)\alpha(T/(Z-1)^2, 1).$$

There is good agreement between the present results and those of Mewe and Schrijver for 2 ^1P and 2 ^3S, but some differences are present in for the 2 ^3P term as well as the systematic factor of 3 discrepancy for the 2 ^1S term. On the other hand, the hydrogenic extrapolation of the rate coefficients reproduces very well the recombination rates for 2 ^1S and 2 ^3S but it systematically overestimates the rate coefficients for the 2 ^1P and 2 ^3P terms. For the latter term, the hydrogenic extrapolation and the results of Mewe and Schrijver are almost indistinguishable.

It is important to note that the 2 ^3S level is responsible for the well known forbidden (f) line of He-like ions which is used in density and temperature line ratio diagnostics (see Section 5.2). Furthermore, the overestimation of the effective recombination rate to this level by MS yields erroneous diagnostics.

5.2. Density and Temperature Diagnostics

The emission lines that originate from transitions from n=2 levels to the ground state are the most intense in the spectra of He-like ions. These are three resolvable features in medium resolution spectra, i.e. the forbidden (f) 2 $^3S - 1$ ^1S, intercombination (i) 2 $^3P - 1$ ^1S, and resonant (r) 2 $^1P - 1$ ^1S transitions. Strictly speaking, the i feature is composed of two fine structure lines, i.e. 2 $^3P_2 - 1$ $^1S_0$ and 2 $^3P_1 - 1$ $^1S_0$. Historically, these lines are also referred to as x and y lines, and the f and r lines are also called z and w.

Under collisional ionization conditions line ratios among the f, i, and r features are useful density and temperature diagnostics. In photoionized plasmas, however, these diagnostics are misleading (Section 5.3). The intensity ratio $R = I_f/I_i$ is sensitive to

electron density above a critical value. This is because while the $2\ ^3S$ and 2^3P states are populated at nearly constant proportions for a wide rage of conditions the population of $2\ ^3S$ can be excited to the $2\ ^3P$ state for densities such $C(2\ ^3S - 2\ ^3P)N_e \geq A(2\ ^3S - 2\ ^1S)$. The ratio $G = (I_f + I_i)/I_r$ is particularly sensitive to temperature. This is because at high temperatures all the lines are mostly collisionally excited, but at lower temperatures recombination dominates the population of the triplet states.

Blends of satellite lines with the f and i lines complicate the picture as they too have a temperature dependence. The satellite lines come from transitions of the type $1s^2nl - 1s2snl$. Dielectronic recombination is the most important excitation mechanism for the majority of these lines, but for some satellites collisional inner-shell excitation is important. The intensity ratio of dielectronic satellites to the the r line is roughly proportional to T^{-1}.

Fig. 3 shows the R ratios vs. N_e for several ions. The density sensitivity of the R ratios starts at around 10^9 cm^{-3} for O VII and around 10^{16} cm^{-3} for Fe XXV. The systematic behavior of the R and G ratios along the helium isoelectronic sequence were explored by Pradhan (1982). Under low density conditions the R ratios exhibit a relatively weak temperature dependence.

G ratios vs. temperature plots are shown in Fig. 4 (solid curves). These ratios present strong temperature dependence which makes them good temperature diagnostics. Also in this plots we show the ratios when the satellite contributions are included (dashed curves). These satellite lines lie to the blue side but very close to the f and i lines. Thus satellites will enhance the apparent G ratio as measured in low to medium resolution spectra. As a consequence, neglecting the contributions of unresolved satellites in the spectra may result in underestimation of the temperature by up to one order of magnitude.

5.3. Emission from Photoionized Plasmas

The traditional line ratio diagnostics discussed above are only applicable to coronal plasmas. On the other hand, photoionization may be the dominant ionization mechanism in a variety of astronomical plasmas. The nature of the ionization mechanism (photoionization or collisional ionization) of the observed plasma must be established before diagnostics can be performed. Fig. 4 shows the G ratio vs. temperature under photoionization conditions (dotted curves). It can be seen that observed ratio from photoionized plasmas departs considerably from that in the coronal case indicated by the solid curve. Thus, failure to recognize photoionization contributions to the emitted spectra will result in misleading diagnostics.

Direct evidence of photoionized plasmas can be found in the strength of lines from the $n = 3$ levels. The strongest of these lines are: $3\ ^1P - 1\ ^1S$ and $3\ ^3D - 2\ ^3P$. Table 1 compares the relative strengths of these lines to the r line in a coronal and photoionized plasmas. The results are given for a 2×10^6K coronal plasma, near the temperature of maximum O VII abundance, and at a temperature of 10^5K, near the thermal equilibrium temperature, for a photoionized plasma. In general, lines from $n = 3$ levels are very weak or undetectable in coronal plasmas, while photoionized plasmas do produce these lines with strengths of up to $\sim 25\%$ of the r line.

Under photoionization conditions a good temperature diagnostic can be obtained from the ratio $I(3\ ^1P - 1\ ^1S)/I(3\ ^3D - 2\ ^3P)$ (P ratio hereafter). This ratio is plotted against temperature in Fig. 5. This ratio conforms a reliable diagnostic without blending with satellite lines and with very high critical densities for collisional deexcitation.

6. Conclusions

We have carried out detailed calculation of recombination spectra of the He-like ions He I, C V, N VI, O VII, Ne IX, Mg XI, Si XIII, S XV, Ar XVII, Ca XIX, and Fe XXV. The calculations include radiative and dielectronic recombination, collisional ionization and three-body recombination, and the effects of high density lowering of the continuum.

These calculations allow us to build ionization-excitation-spectral models for fast computation of the spectra for modeling and/or spectral diagnostics. This models include all levels up to $n = 5$ and the most important satellite lines to the H-like spectra. The IES models are applicable to densities of up to 10^{18} cm^{-3} and converge to LTE under proper conditions.

The results of the IES models are compared with calculations by other authors. It is found the present effective recombination rates differ significantly from earlier estimates by Mewe and Schrijver (1978a). For example, we find that the Mewe and Schrijver recombination rates for the $2\ ^1S$ state are overestimated by a factor of three. The $2\ ^1S$ level decays to the ground state either two-photon continuum or collisional transitions. Thus, the discrepancy found in the recombination rates for this level will be important in trying to simultaneously model line and continuum emission. The difference in recombination to the $2\ ^1S$ level may also affect the line emission spectrum under high density or high optical depth conditions where the $2\ ^1S$ level contributes to the population of other levels.

Further, we present several line ratio diagnostics under coronal and photoionization conditions. It is shown that blends of satellite lines with the traditionally studied forbidden and intercombination lines can considerably enhance the apparent G ratio in coronal plasmas. Also, we find that the traditional R and G line ratio diagnostics used for coronal plasmas are misleading when the plasma is photoionized. Such photoionized plasmas can be recognized by the presence of lines arising from n =3 levels in the spectra. Moreover,

these lines can used for reliable temperature diagnostics.

The present IES models, data files and a computer code, is available upon request to the authors. These models can be implemented in spectra modeling codes or used as a stand alone tool for spectral diagnostics. In this sense, the present IES models for He-like ions and similar ones for H-like (Bautista et al. 1998) are already implemented in the photoionization modeling code XSTAR v.2 (Kallman and Bautista 2000). For isoelectronic sequences other than H and He-like XSTAR v.2 accounts only for direct recombination to every level, but calculations of more detailed recombination models like those described in this paper are underway.

Acknowledgments

This work has been supported in part by a grant from the Smithsonian Observatory for the Emission Line Project.

Table 1. Line intensities relative to the r line for coronal and photoionized O VII

Transition	Coronal (T=2×10^6K)	Photoionized (T=10^5K)
$2\ ^1P - 1\ ^1S$	1.0	1.0
$2\ ^3S - 1\ ^1S$	0.57	3.47
$2\ ^3P - 1\ ^1S$	0.16	0.98
$3\ ^3P - 2\ ^3S$	0.002	0.10
$3\ ^3D - 2\ ^3P$	0.001	0.27
$3\ ^1P - 1\ ^1S$	0.014	0.20

REFERENCES

Badnell, N.R. et al. 1995, AIP Conference Proceedings 322, 84 (ADAS).

Almog, Y. and Netzer, H. 1989, MNRAS, 238, 57.

Bhatia, A.K. and Underhill, A.B. 1986, ApJS60, 323

Bautista, M.A. 2000, J. Physics B. At. Mol. Opt. Phys. 33, 71.

Bautista, M.A., Kallman, T.R., Angelini, L., Liedahl, D.A., and Smits, D.P. 1998, ApJ, 509, 848

Benjamin, R.A., Skillman, E.D., and Smits, D.P. 1999, ApJ, 314, 307

Brocklehurst, M. 1971, MNRAS153, 471

Burgess, A. & Seaton, M.J. 1960a, MNRAS, 120, 121

—, 1960b, MNRAS, 121, 471

Burgess, A. & Summers, H.P. 1969, ApJ, 157, 1007

—, 1976, MNRAS, 174, 345

Cota, S.A. 1987, Ph.D. thesis, Ohio State Univ.

Cunto, W., Mendoza, C., Ochsebein, F., and Zeippen, C.J. 1993, A&A275, L5

Drake, G.W.F. 1969, ApJ, 158, 1199

—, 1971a, Phys. Rev. A, 3, 908

—, 1971b, ApJ, 163, 439

Drake, G.W.F. and Dalgarno, A. 1969, ApJ, 157, 459

Dubau, J. 1994, Atomic Data and Nucl. Data Tables, 57, 21

Ferland, G.J. 1993, University of Kentucky Department of Physics and Astronomy Internal Report.

Fernley, J.A., Taylor, K.T., and Seaton, M.J. 1987, J. Physics B. At. Mol. Opt. Phys., 20, 6457.

Gabriel, A.H. and Jordan, C. 1969, MNRAS, 145, 241

—, 1970, Phys Letters (Neth.) 32A, 166

—, 1972, "case Studies in Atom. Collision Phys 2, eds. E.W. McDaniel and M.R.C. McDowell, North Holland Pub. Co. Amsterdam, p.209

—, 1973, ApJ186, 327

Goett, S.J., Sampson, D.H., and Clark, R.E.H. 1983, Atomic Data and Nuclear Data Tables, 28, 279.

Hahn, Y. 1997, Physics Letters A, 231, 82.

Hummer, D.G. and Storey, P.J., 1987, MNRAS, 224, 801.

Hummer, D.G. and Storey, P.J. 1998, MNRAS, 297, 1073.

Inglis, D.R. & Teller, E. 1939, ApJ, 90, 439.

Johnson, W.R. and Lin, Chieng-Ping 1974, Phys. Rev. A, 9, 1486

Jordan, C. 1969, MNRAS, 142, 301

Kallman, T.R. & Bautista, M.A. 2000, ApJ(submitted).

Kallman, T.R. & Krolik J.H. 1994, NASA/GSFC/LHEA preprint

Kato, T. and Nakazaki, S. 1989, Atomic Data and Nucl. Data Tables, 42 313

Kono, A. and Hattori, S. 1984, Phys. Rev. A, 29 2981

Mathis, J. 1957, ApJ, 125, 318

Mewe, R. & Schrijver, I. 1978a, A&A65, 99

Mewe, R. & Schrijver, I. 1978b, A&A65, 115

Mewe, R. & Schrijver, I. 1978c, A&AS33, 311

Nahar S.N. and Pradhan, A.K. 1999, A&AS, 135, 347

Nayakshin, S., Kazanas, D., and Kallman, T.R. 2000, ApJ, in press

Martin, W.C., Sugar, J., and Musgrove, A. 1999, "NIST Atomic Spectroscopic Data v.2: Atomic Energy Levels and Wavelengths", URL: physics.nist.gov/sgi-bin/AtData

Osterbrock, D. E. 1989, *Astrophysics of Gaseous Nebula and Active Galactic Nuclei* (Mill Valley: University Science Books).

Pottasch, S.R. 1962, ApJ, 135, 385

Pradhan, A.K. 1982, ApJ, 263, 479

—, 1985, ApJ288, 824

Pradhan, A.K. and Shull, J.M. 1981, ApJ249, 821

Robbins, R. 1968, ApJ, 151, 497

—, 1970, ApJ, 160, 519

Robbins, R. and Robinson, E.L. 1971, ApJ, 167, 249

Sampson, D.H., Goett, S.J., and Clark, R.E.H. 1983, Atomic Data and Nuclear Data Tables, 28, 299.

Sampson, D.H. and Zhang, H.L. 1988, ApJ, 335, 156.

Seaton, M.J. 1962, Proc. Phys. Soc., 79, 1105

—, 1987, J. Physics B. At. Mol. Opt. Phys., 20, 6363

Smits, D.P. 1991, MNRAS, 248, 193.

Smits, D.P. 1996, MNRAS, 278, 683

Summers, H.P. 1972, MNRAS, 158, 255

Vainshtein, L.A. & Safronova, D.J. 1978, Atomic Data and Nucl. Data Tables, 21, 49.

This manuscript was prepared with the AAS LaTeX macros v4.0.

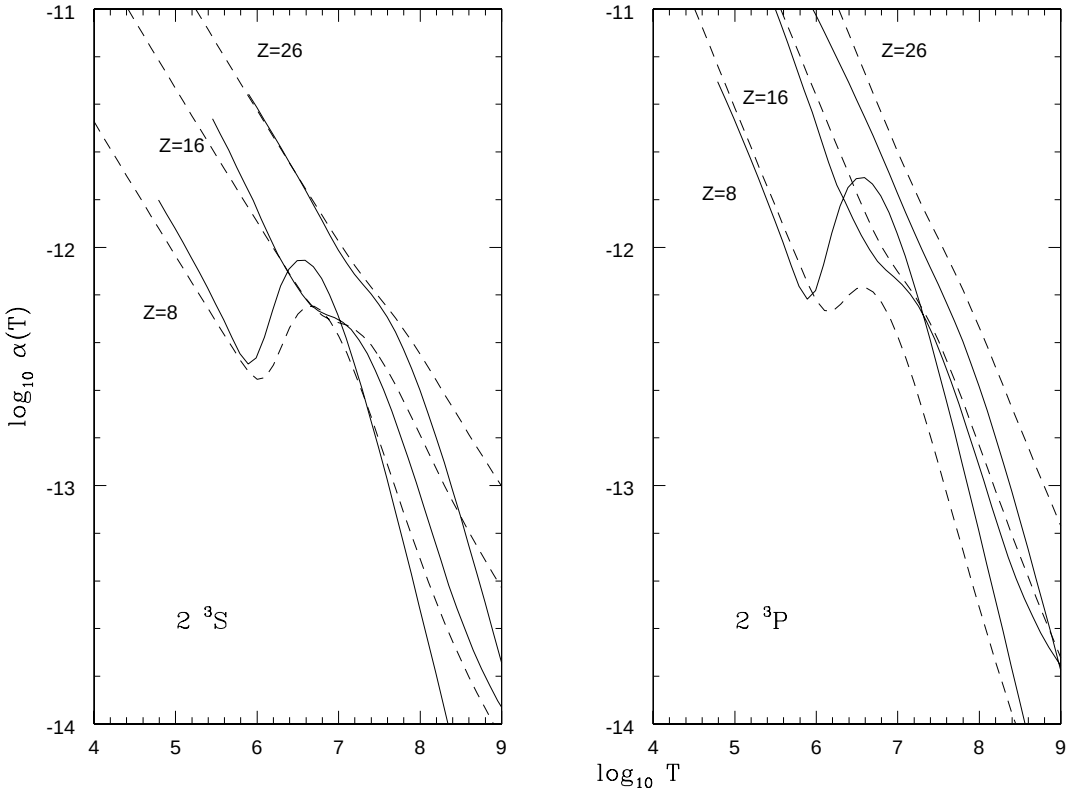

Fig. 1.— Comparison of effective recombination rate coefficients (direct recombination and cascades) against temperature for $n = 2$ term between present calculations (solid lines) and estimates by Mewe and Schrijver (1978; dashes lines).

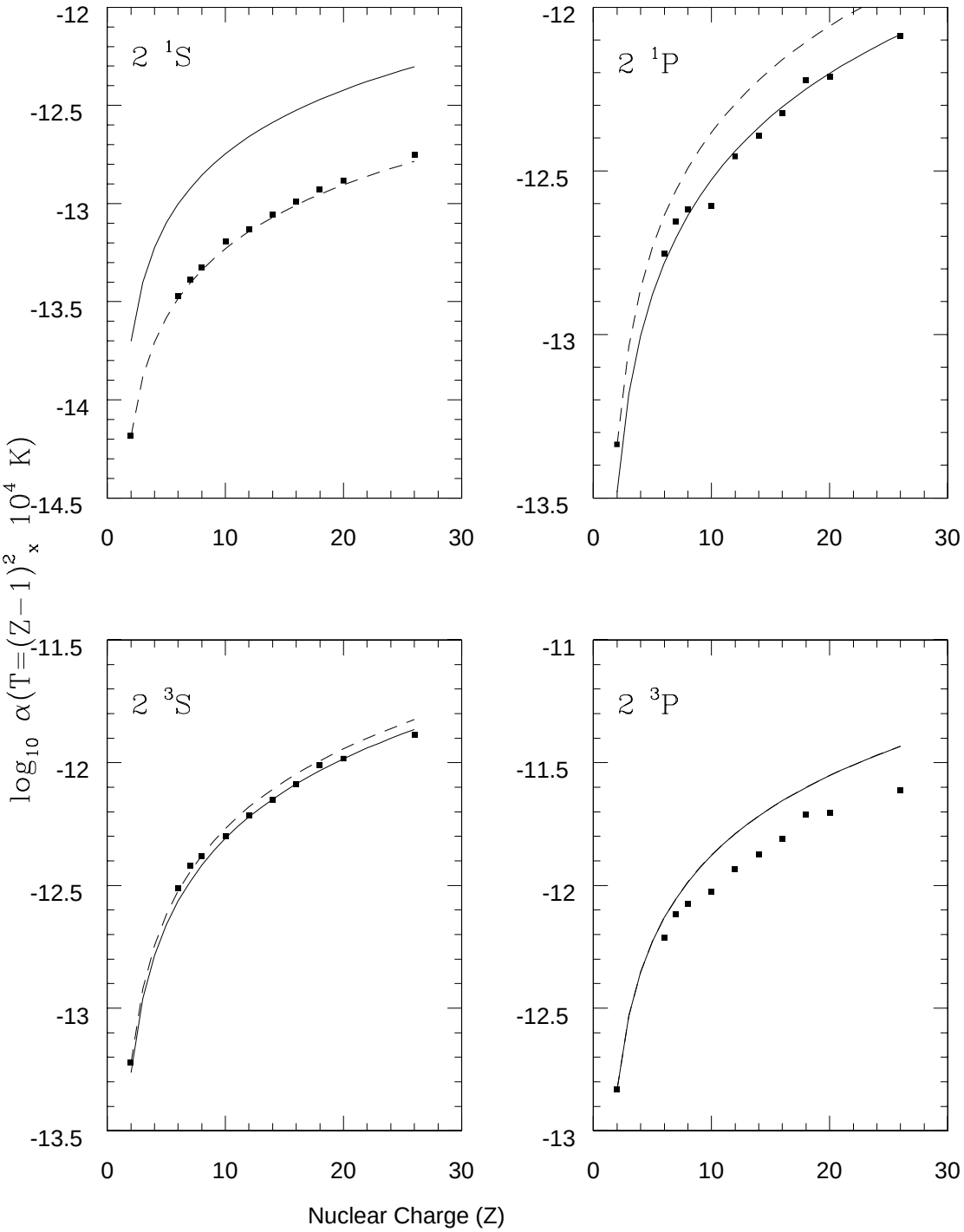

Fig. 2.— Effective recombination coefficients at T=$10^4\times$(Z-1)^2 K vs. nuclear charge Z. The square points represent the present results, the solid lines represent the estimates of Mewe and Schrijver (1978), and the dashed lines are hydrogenic extrapolations of rate coefficients from He I (see text).

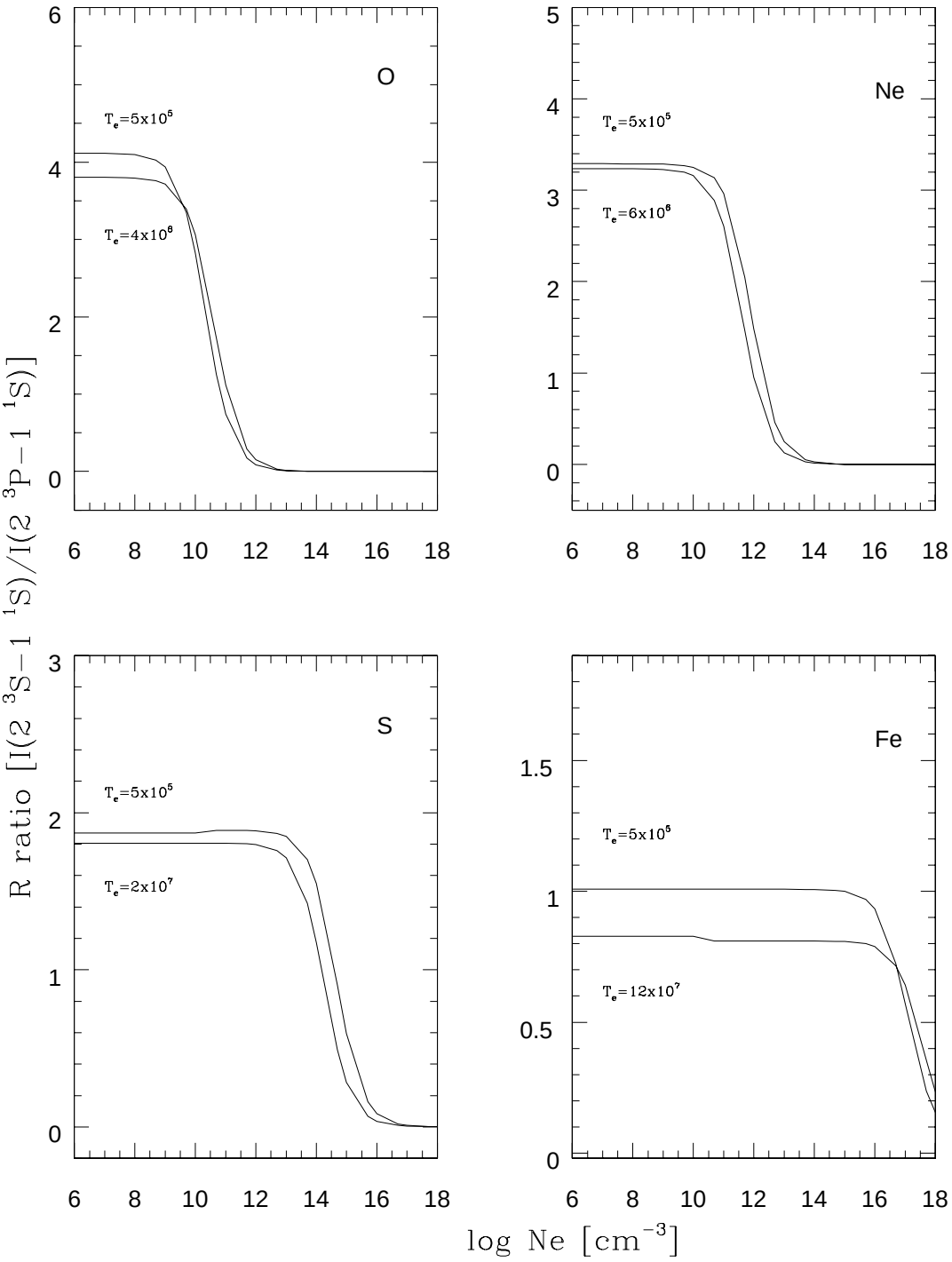

Fig. 3.— The R ratios (forbidden to intercombination line intensity ratios) vs. electron density.

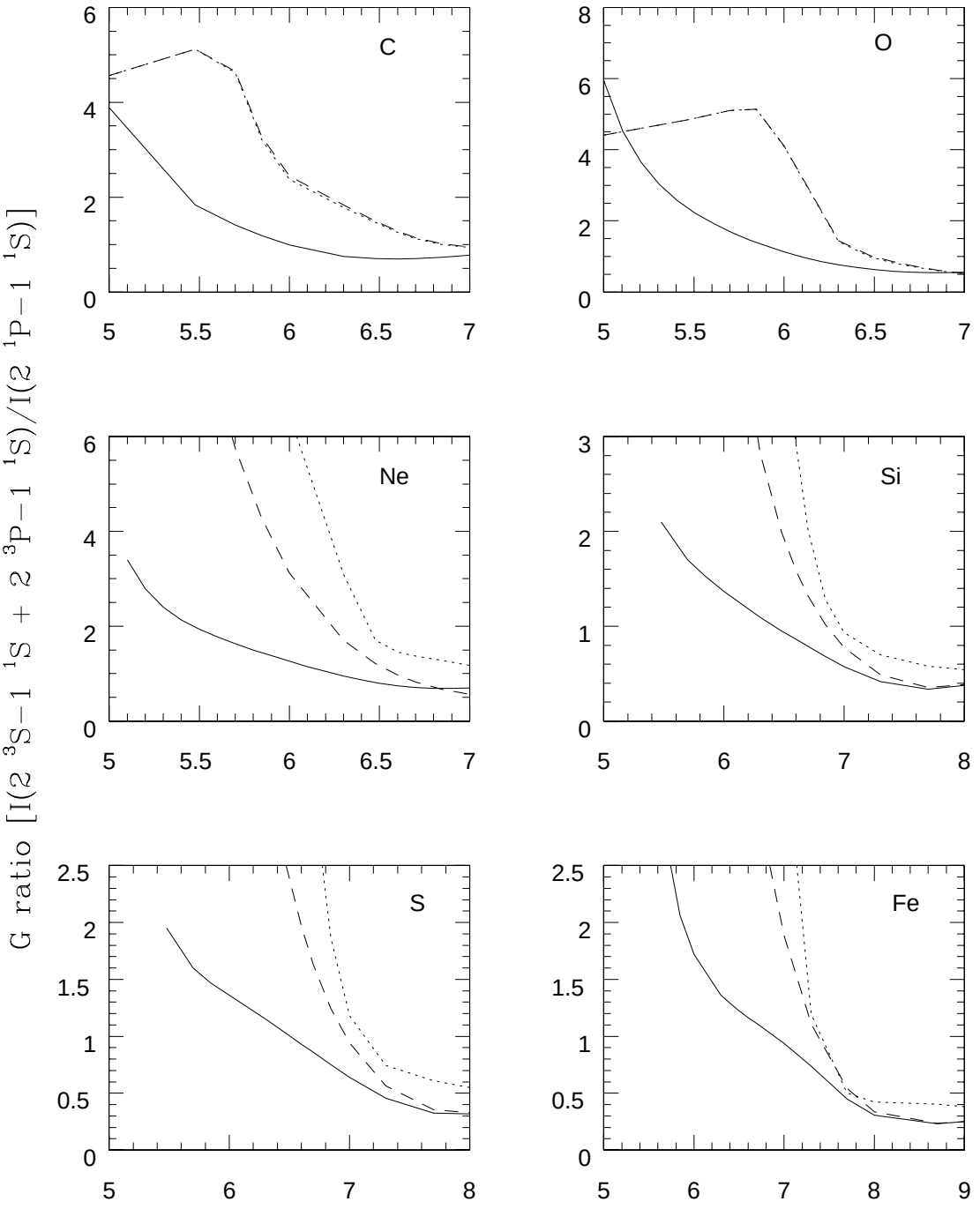

Fig. 4.— The G ratios (forbidden plus intercombination to resonant line intensity ratios) vs. temperature. The solid curves represent the the ratios under coronal ionization conditions. The dashed lines show the ratios including satellites line contributions. The dotted lines represent the G ratios under photoionization conditions.

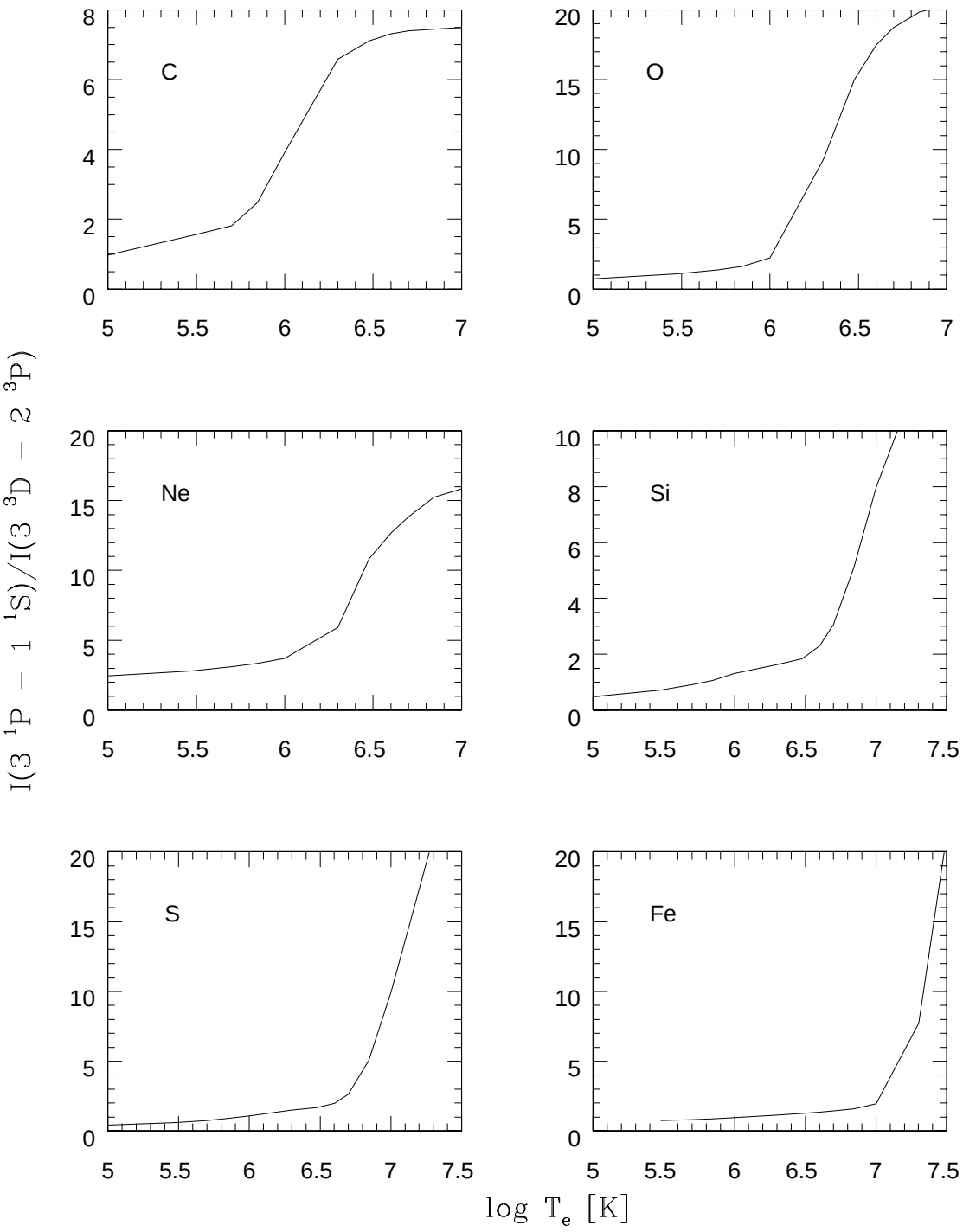

Fig. 5.— The P ratios ($I(3\ ^1P - 1\ ^1S)/I(3\ ^3D - 2\ ^3P)$) vs. temperature.